PCCP

ARTICLE TYPE

Cite this: DOI: 00.0000/xxxxxxxxxx

Theoretical investigation of enhancement of positron affinity by vibration and dimerization of non-polar carbon disulfide†

Miku Furushima,[a] Daisuke Yoshida,*[a] Yukiumi Kita,*[b] Tomomi Shimazaki,[a] and Masanori Tachikawa*[c]

Received Date
Accepted Date

DOI: 00.0000/xxxxxxxxxx

Available from : https://pubs.rsc.org/en/content/articlelanding/2021/cp/d1cp02808a

The positronic bound state for the non-polar carbon disulfide (CS_2) was experimentally identified, while previous theoretical investigations, which dedicated to studying the positronic CS_2 monomer, cannot reasonably reproduce the experimentally measured positron affinity. In the present study, we performed analysis of the vibrational averaged positron affinity for the positronic CS_2 dimer, [C_2S_4; e^+], using the Hartree-Fock and configuration interaction level of multi-component molecular orbital method combined with the self-consistent field level of vibrational variational Monte Carlo method. We obtained that the equilibrium structure of the non-polar C_2S_4 can have the positronic bound state with the positron affinity of about 46.18 meV in configuration interaction level while 0 meV in Hartree-Fock level. Furthermore, by taking into account the vibrational effect, we succeeded in reproducing the resonant positron kinetic energies lying close to the experimental value, where the vibrational averaged positron affinity becomes greater with increased dipole moment and dipole polarizability. We also showed possible mechanisms effectively to enhance the resonant positron capture for [C_2S_4; e^+], associated with both infrared active and infrared inactive vibrational modes.

1 Introduction

Positron interactions with the molecule have been studied due to interests in many fields, such as, fundamental antimatter physics and chemistry[1,2], molecular and materials science[3,4], biomedical applications[5,6], and so on. In particular, low energy positron ionization technique for organic molecules has the potential to realize new field of mass spectromerty[3]. In the last few decades, both theoretical and experimental sides as well as their combined approach have provided evidences for the existence of the (metastable) positron–molecule bound states for the various complex species. The low-energy positron beam technique, which has been developed by Surko's group, have successfully measured the positron annihilation spectra and identified the positron–molecular complexes for a number of molecular species[7–12], involving some weakly- and non- polar molecular species. Gribakin and Lee have developed a practical theory systematically to describe the observed annihilation spectra based on the resonant mechanism for the positron capture[13,14]. Their theoretical description combined with the experimental simulations obtained the important chemical trends related to the molecular electrostatic properties: for non-polar or weakly-polar molecules, the dipole polarizability becomes an important parameter[15,16] concerning the dipole field induced by the positron attachment, while for strongly-polar molecules, the permanent dipole moment also has a significant contribution to the positron binding[17]. The *ab initio* theoretical studies have performed the direct calculations of the positron binding energy (the positron affinity, PA) mostly for the polar molecules or clusters, such as, for example, cyanides[18,19], nitriles[20], biological molecules[21,22], hydrated clusters[23] and so on. Several years ago, the positron resonant annihilation on the non-polar CS_2 molecule was observed experimentally[24], where positron beam with the kinetic energy 115 meV shows resonance peak and this result was interpreted that CS_2 has the positronic bound state with the positron binding energy of 75 meV. *Ab initio* theoretical studies has attempted to reproduce the experimental data to figure out the positron binding mechanism; immediately, the positron binding ability of the CS_2 monomer was investigated, and the direct calculation for the positron affinity provided almost zero at the equilibrium CS_2

[a] *Quantum Chemistry Division, Yokohama City University, Seto 22-2, Kanazawa-ku, Yokohama 236-0027, Kanagawa, Japan. Fax: +81-45-787-2188; Tel: +81-45-787-2188; E-mail: daiy@yokohama-cu.ac.jp*

[b] *Quantum Chemistry Division, Yokohama City University, Seto 22-2, Kanazawa-ku, Yokohama 236-0027, Kanagawa, Japan. Fax: +81-45-787-2188; Tel: +81-45-787-2188; E-mail: ykita@yokohama-cu.ac.jp*

[c] *Quantum Chemistry Division, Yokohama City University, Seto 22-2, Kanazawa-ku, Yokohama 236-0027, Kanagawa, Japan. Fax: +81-45-787-2188; Tel: +81-45-787-2188; E-mail: tachi@yokohama-cu.ac.jp*

† Electronic Supplementary Information (ESI) available: See DOI: 10.1039/cXCP00000x/

molecule. This result predicts not to form a positronic bound state and is quite in disagreement with the experimental fact. Furthermore, the vibrational averaged PA was analyzed to take the effect of the vibrationally induced dipole moment into account[25]. This work offered us that vibrationally excited states have a crucial role to enhance the positron affinity for the non-polar CS_2 system, but the vibrational averaged PA of about 2–5 meV was too small to rationalize the experimental results and corresponding resonance positron kinetic energy estimated is 190 meV, which is far from experimental result 115 meV. Thus, early theoretical studies with focus on the individual CS_2 molecule failed in quantitativity, and the issue for the positron binding ability of the gas-phase CS_2 still remains an open question. In more recent years, importantly, the carbon disulfide dimer C_2S_4 and trimer C_3S_6 were observed in gas-phase by pulsed supersonic slit-jet experiments[26,27]. The positron interacting with such CS_2 clusters may be invoked for the feasibility for the existence of the positronic carbon disulfide complex.

In the present study, we investigate the positron binding ability of C_2S_4 in compared to that of CS_2 by means of the *ab initio* theoretical method. In order to figure out the dynamical effect to the positron binding ability of C_2S_4, we calculate the vibrational averaged PA for the dimer by applying the multi-component molecular orbital (MC_MO) method combined with the variational Monte Carlo method to solve the (excited) vibrational state wave functions. We describe the important definition equation and the *ab initio* method we applied in the following section.

2 Theory

2.1 Vibrational averaged PA and other properties

On the basis of the vibrational Feshbach resonance (VFR) for the positron attachment to the molecule[13,14], the resonant positron kinetic energy K_ν can be evaluated by

$$K_\nu = E_\nu - \mathrm{PA}_\nu, \tag{1}$$

where E_ν is the excitation energy from vibrational ground state to ν-th vibrational excited state and PA_ν is the positron affinity of ν-th vibrational excited state. In this work, we obtain the vibrational eigenstates for a molecule by adopting the rovibrational Hamiltonian by Watson[28], and seek PA values depending on the molecular vibrational states. PA_ν is represented by vibrational averaged scheme as follows. For arbitrary property A, vibrational averaged property A_ν is defined as,

$$A_\nu = \frac{\int A(\boldsymbol{Q})|\Psi_\nu(\boldsymbol{Q})|^2 \,\mathrm{d}\boldsymbol{Q}}{\int |\Psi_\nu(\boldsymbol{Q})|^2 \,\mathrm{d}\boldsymbol{Q}}, \tag{2}$$

where $A(\boldsymbol{Q})$ is scalar property at the geometry of $\boldsymbol{Q}$ and $\Psi_\nu(\boldsymbol{Q})$ is the vibrational wavefunction. This equation means weighted average of A using a weight with $|\Psi_\nu(\boldsymbol{Q})|^2$.

Vibrational averaged property of single mode ν_i is also important and defined as

$$A_{\nu_i} = \frac{\int A(Q_i)|\Psi_\nu(Q_i)|^2 \,\mathrm{d}Q_i}{\int |\Psi_\nu(Q_i)|^2 \,\mathrm{d}Q_i}, \tag{3}$$

where Q_i is the i-th normal vibrational coordinate. $\mathrm{PA}(\boldsymbol{Q})$ is defined as

$$\mathrm{PA}(\boldsymbol{Q}) = E^{[\mathrm{A}]}(\boldsymbol{Q}) - E^{[\mathrm{A};\mathrm{e}^+]}(\boldsymbol{Q}), \tag{4}$$

where $E^{[\mathrm{A}]}(\boldsymbol{Q})$ and $E^{[\mathrm{A};\mathrm{e}^+]}(\boldsymbol{Q})$ are the total energies at the normal mode coordinates $\boldsymbol{Q}$ for the parent molecule A and its positronic compound $\left[\mathrm{A};\mathrm{e}^+\right]$, respectively. The leptonic state at the fixed nuclear configuration is obtained by solving the leptonic Schrödinger equation $\hat{H}_{\mathrm{lep}}\Psi(\boldsymbol{r};\boldsymbol{Q}) = E_{\mathrm{lep}}\Psi(\boldsymbol{r};\boldsymbol{Q})$, and the vibrational states is obtained by solving the Schrödinger equation for the vibrational nuclear motions with the effective Hamiltonian $\hat{H}_{\mathrm{vib}}$, i.e., the eigenvalue equation as $\hat{H}_{\mathrm{vib}}\Psi_\nu(\boldsymbol{Q}) = E_\nu\Psi_\nu(\boldsymbol{Q})$.

2.2 Multi-component molecular orbital method

For the calculation of the total energy for the leptonic system, we used the MC_MO method[29]. The non-relativistic leptonic Hamiltonian for the system containing N_e electrons, N_{nuc} nuclei, and a positron is written as

$$\begin{aligned}\hat{H}_{\mathrm{lep}} = \quad & -\frac{1}{2}\sum_i^{N_\mathrm{e}}\boldsymbol{\nabla}_i^2 - \frac{1}{2}\boldsymbol{\nabla}_p^2 \\ & + \sum_i^{N_\mathrm{e}}\sum_{j>i}^{N_\mathrm{e}}\frac{1}{r_{ij}} - \sum_i^{N_\mathrm{e}}\sum_I^{N_{\mathrm{nuc}}}\frac{Z_I}{r_{iI}} - \sum_i^{N_\mathrm{e}}\frac{1}{r_{ip}} + \sum_I^{N_{\mathrm{nuc}}}\frac{Z_I}{r_{pI}},\end{aligned} \tag{5}$$

where the first and the second terms are the kinetic energy operators for the electrons and the positron, respectively, the other terms are the Coulomb interactions: Z_I is the charge of the I-th nucleus and r_{ij}, r_{ip}, *etc.* are the interparticle distances. The configuration interaction (CI) expansion for the multi–component wave function can be represented as $|\Psi^{\mathrm{CI}}\rangle = \sum_{L_\mathrm{e},L_\mathrm{p}}|\Phi^\mathrm{e}_{L_\mathrm{e}}\rangle|\Phi^\mathrm{p}_{L_\mathrm{p}}\rangle C_{L_\mathrm{e}}C_{L_\mathrm{p}}$, where C_{L_x} is the L_x-th CI coefficient for L_x–th configuration, $\Phi^x_{L_x}$, for the particle kind x; $x = \mathrm{e}$ (electron) and p (positron). The CI energy, E^{CI} is written as

$$E^{\mathrm{CI}} = \sum_{L_\mathrm{e},L_\mathrm{p}}\sum_{L'_\mathrm{e},L'_\mathrm{p}} C_{L_\mathrm{e}}C_{L'_\mathrm{e}}C_{L_\mathrm{p}}C_{L'_\mathrm{p}}\langle\Phi^\mathrm{p}_{L_\mathrm{p}}|\langle\Phi^\mathrm{e}_{L_\mathrm{e}}|\hat{H}_{\mathrm{lep}}|\Phi^\mathrm{e}_{L'_\mathrm{e}}\rangle|\Phi^\mathrm{p}_{L'_\mathrm{p}}\rangle. \tag{6}$$

In above formalism, if we consider only the first term of the CI wave function with $C_{L_\mathrm{e}}C_{L_\mathrm{p}} = 1$, we can derive the Hartree-Fock (HF) equation of the multi-component molecular orbital method, and then the HF total energy is given by $E^{\mathrm{HF}} = \langle\Phi^\mathrm{p}_0|\langle\Phi^e_0|\hat{H}_{\mathrm{lep}}|\Phi^\mathrm{e}_0\rangle|\Phi^\mathrm{p}_0\rangle$. We utilized the McMurchie-Davidson method[30] for integral calculations, and applied the graphical unitary group approach (GUGA) technique[31] to evaluate the CI matrix elements in Eq. (6).

Parent molecule absolute dipole moment μ and isotropic dipole polarizability α are calculated by HF method and vibrational averaged values of them are estimated by Eq.2 . Here, isotropic dipole polarizability $\alpha = \left(\alpha_{xx} + \alpha_{yy} + \alpha_{zz}\right)/3$, where x, y, and z denote the axes of cartesian coordinate system and α_{ii}s correspond to the polarize property along i-direction under applied electronic-field in the i-direction.

2.3 Vibrational variational Monte Carlo method

The vibrational wave function for the parent molecule A was resolved in the adiabatic approximation via the Hamiltonian by

Watson[28], where the eigenfunction for the system $\Phi_\nu(\boldsymbol{r},\boldsymbol{R})$ can be separable into the vibrational wave function and the (static) electronic wave function at the fixed nuclei:

$$\Phi_\nu(\boldsymbol{r},\boldsymbol{R}) = \Psi_\nu^{\rm vib}(\boldsymbol{R})\cdot\Psi^{\rm e}(\boldsymbol{r};\boldsymbol{R}), \tag{7}$$

where the suffix for the eigenstate of the leptonic part is omitted, and the external potential energy is formed by the electronic wave function $\Psi^{\rm e}(\boldsymbol{r};\boldsymbol{R})$. We used the vibrational self-consistent field (VSCF) method to obtain the vibrational eigenstates, $|\Psi_\nu^{\rm vib}(\boldsymbol{Q})\rangle$. The trial vibrational wave function within the constraint of the single Hartree product is given by a product of the modal functions,

$$\Psi_\nu^{\rm vib}(\boldsymbol{Q}) = \prod_{i=1}^{M}\psi_{\nu_i}(Q_i), \tag{8}$$

where M is the number of the vibrational modes, and $\psi_{\nu_i}(Q_i)$ is the i-th single-mode wavefunction. $\psi_{\nu_i}(Q_i)$ may be expressed as a linear combination of the mode-specific basis functions $\chi_n^{(i)}(Q_i)$:

$$\psi_{\nu_i}(Q_i) = \sum_{n=1}^{N_i} C_n^{(i)}\chi_n^{(i)}(Q_i), \tag{9}$$

with the expansion coefficients $\{C_n^{(i)}\}$. In this work, we adopted the harmonic oscillator functions as the basis functions $\chi_n^{(i)}(Q_i)$:

$$\chi_n^{(i)}(Q_i) = h_{n-1}\left(\sqrt{\varepsilon^{(i)}}(Q_i - Q_c^{(i)})\right)\exp\left(-\frac{\varepsilon^{(i)}}{2}(Q_i - Q_c^{(i)})^2\right), \tag{10}$$

where $h_n(\xi)$ is the n-th Hermite polynomial, and Q_i is the i-th (generalized) internal coordinate corresponding to the center of the harmonic oscillator in the basis function. By optimizing the trial wave function Eq.(8), we obtain the energy eigenvalue for the vibrational state ν, described as

$$E_\nu = \frac{\langle\Psi_\nu^{\rm vib}|\hat{H}_{\rm vib}|\Psi_\nu^{\rm vib}\rangle}{\langle\Psi_\nu^{\rm vib}|\Psi_\nu^{\rm vib}\rangle} = \frac{\int E_L(\boldsymbol{Q})|\Psi_\nu^{\rm vib}(\boldsymbol{Q})|^2{\rm d}\boldsymbol{Q}}{\int|\Psi_\nu^{\rm vib}(\boldsymbol{Q})|^2{\rm d}\boldsymbol{Q}}, \tag{11}$$

where $\hat{H}_{\rm vib}$ is the rovibrational Hamiltonian by Watson[28], and $E_L(\boldsymbol{Q}) = \Psi_\nu(\boldsymbol{Q})^{-1}\hat{H}_{\rm vib}\Psi_\nu(\boldsymbol{Q})$ is the local energy.

In our VSCF calculation, the vibrational states are resolved by fulfilling the fully-variational optimization for the modal wave functions $\psi_{\nu_i}(Q_i)$, i.e., all the variational parameters, $C_n^{(i)}$, $\varepsilon^{(i)}$, and $Q_c^{(i)}$ are optimized, as minimizing the expectation value of the local energy $E_{\rm L}(\boldsymbol{Q})$ by the variational Monte Carlo technique in cooperation with the linear optimization method[32].

3 Computational details

In order to figure out the positron binding abilities of the equilibrium CS_2 dimer, we first calculated the vertical PA values at the equilibrium geometries. The geometry optimizations were performed using the coupled cluster singles and doubles (CCSD) method with Dunning's augmented correlation-consistent polarized valence double zeta (aug-cc-pVDZ) basis set for CS_2 dimer. The geometry optimization were performed using Gaussian 16 package[33].

The leptonic total energies for both positronic compounds within the Born-Oppenheimer approximation were calculated using both HF and CI singles and doubles (CISD) levels of the MC_MO framework, where CISD in this work stands for the configuration interactions arising from single electronic, single positronic, and both single electronic–single positronic excitations to take account of the important electron–positron correlation effect. We employed the 6-31+G($2df$) basis set and [$1s1p$] Gaussian type diffuse functions for the electrons, where the exponents of 0.06 were chosen for the [$1s1p$] diffuse functions. For the positronic part, we employed [$18s15p6d4f2g$] Gaussian type functions (GTFs): [$6s5p6d4f2g$], [$4s3p$], and [$1s1p$] are located at the center of mass, two carbon nuclei, and four sulfur nuclei, respectively. These exponents were determined by the even-tempered scheme, $\alpha_{i+1} = c\times\alpha_i$ with $c=\sqrt{10}$, where $\alpha_1 = \sqrt{10}\times10^{-4}, \sqrt{10}\times10^{-3}, \sqrt{10}\times10^{-3}$, $\sqrt{10}\times10^{-2}$, and $\sqrt{10}\times10^{-2}$ for s-, p-, d-, f-, and g- type functions of [$6s5p6d4f2g$], respectively, $\alpha_1 = 0.1$ for both s- and p- type functions of [$4s3p$], and $\alpha_1 = 1$ for both s- and p- type functions of [$1s1p$]. Both HF and CI calculations of MC_MO were performed using FVOPT program[29]. In the VSCF procedure for the CS_2 dimer, the normal mode vibrational coordinates $\boldsymbol{Q}$ are obtained by harmonic analysis via the same level of *abinitio* calculations as the geometry optimizations. The CS_2 dimer has twelve normal vibrational modes as shown in Table 1, where ν_i represents the vibrational quantum number for the i-th normal mode vibration. We show schematic representations for the vibrational modes, particularly, ν_1, ν_9, ν_{10}, and ν_{11}, which are considered to mainly contribute to the vibrational resonant positron capture to be discussed in the following discussion. The global potential energy surface (PES) of CS_2 dimer is calculated by interpolating potential energy values at discrete grid points in vibrational configuration space expanded with the normal mode vectors. In principle, a twelve-dimensional PES is required to take all inter-mode couplings between modes into accounts for this molecule. High-dimensional couplings in PES, however, generally give negligible contributions despite tremendous computational costs. To reduce computational costs, we used the n-mode representation technique proposed by Carter et al.[34], in which the approximate PES is expressed by truncating higher-order coupling terms. To construct an approximate PES for CS_2 dimer, we employed the three-mode representation including coupling terms up to the second order. The potential energy at each grid point was calculated at the same *abinitio* level as the geometry optimization and normal mode analysis. The total number of grid points is 49969. All the variational parameters of the basis functions were optimized with respect to the ground vibrational state, but only the expansion coefficients were optimized for all the excited vibrational states. All VSCF calculations were performed using our in-house vibrational quantum Monte Carlo program[35].

For evaluations of the resonant positron kinetic energies based on Eq.(1), we mapped vertical PA surface on the normal mode coordinates $\boldsymbol{Q}$ from the total energy maps obtained by CI level calculations with the spline interpolation. In this procedure, appropriate 169 grids were selected to reduce the computational demands.

To understand the effect of $\mu(\boldsymbol{Q}_{\rm eq})$, $\alpha(\boldsymbol{Q}_{\rm eq})$ where $\boldsymbol{Q}_{\rm eq}$ denotes

Table 1 Normal vibrational modes ν_i and corresponding vibrational energies E_{ν_i} and infrared (IR) intensities I_{ν_i} for the CS_2 dimer with CCSD/aug-cc-pVDZ level of calculation. Energies and IR intensities are given in units of cm^{-1} and arb. unit, respectively.

Vibrational mode representation	Vibrational modes	E_{ν_i}	I_{ν_i}
ν_1	Rotational-twisting	15.94	0
ν_2, ν_3	Wagging	32.36	0.01
ν_4	CC intermolecular stretching	44.32	0
ν_5	B_2 symmetric SCS bending	376.13	5.02
ν_6, ν_7	E symmetric SCS bending	379.54	2.88
ν_8	A_1 symmetric SCS bending	380.61	0
ν_9	B_2 symmetric CS stretching	675.53	0.02
ν_{10}	A_1 symmetric CS stretching	675.66	0
ν_{11}, ν_{12}	Asymmetric CS stretching	1540.26	785.12

equilibrium geometry, μ_ν, and α_ν based on Eq.(2), we calculated $\mu(\boldsymbol{Q})$ and $\alpha(\boldsymbol{Q})$ on the normal mode coordinates $\boldsymbol{Q}$ by the HF/6-31+G($2df$) level of calculation. In this procedure, appropriate 49969 grids were selected.

4 Results and Discussion

4.1 Equilibrium structure for positronic CS_2 dimer

The equilibrium structure, the electrostatic molecular properties, and the positron affinity for C_2S_4 are shown in Table 2. Detailed calculation results for the potential energy curves can be found in Figure S1 (ESI†). In order to discuss the positron binding ability for C_2S_4 relative to its constituent monomer CS_2, we here refer to the same properties for CS_2 presented by Takeda *et al.*'s work[25]. The individual CS_2 system has a $D_{\infty h}$ highly symmetric linear geometry, which has no permanent dipole moment μ. As we mentioned above, the equilibrium CS_2 was predicted not to have a positive PA (i.e., no positron binding ability) in the equilibrium state. On the other hand, C_2S_4 has a D_{2d} symmetrical cross-shaped geometry with the equilibrium CC interatomic distance $R_{CC} = 3.65$ Å. Our optimized structure shows reasonable agreement with the experimentally measured CC distance, $R_{CC} = 3.539$ Å[26], and the CS_2–CS_2 intermolecular binding energy $E_{int} = 2.07$ kcal/mol $= 723$ cm^{-1} is also consistent with 773 cm^{-1} resulted from the earlier calculation using the model potential[36]. For the [C_2S_4; e^+] system, HF level calculation predicted PA $= 0$, whereas by inclusion of the electron-positron correlation effect via CI method, PA drastically increases to 46.18 meV. Conventionally, it has been considered that for strongly-polar molecules the large permanent dipole moment is favored in binding a positron, while for non- and/or weakly-polar molecules, the dipole polarizability becomes an important parameter related to the electrostatic field induced by the positron attachment. For the case of C_2S_4, the two times larger dipole polarizability α in compared to CS_2 may play an important role for the ability to bind a positron.

As shown in Table 2, atomic charges obtained by the natural bond orbital analysis are -0.256 for a carbon atom and 0.128 for a sulfur atom for the C_2S_4 system. These charge separations for every CS_2 unit are smaller rather than the individual CS_2 system, but the total charge distribution due to forming the dimer may have an influence on the interaction with a positron. The positron density distribution for the positronic bound state of [C_2S_4; e^+] is shown in Figure 1 (a). The bound positron appears as a saddle-like shape around CS_2–CS_2 intermolecular axis, where indeed, the bound positron seems to evade positively charged sulfur atoms and to extend around negatively charged carbon atoms. Such a positron binding feature looks to be quite different to extents of the (loosely) bound positrons for the positronic polar systems; the positron density maximum tends to be located near the partially negatively charged atom(s) as contributing the gross dipole moment of the parent systems, and the distribution is often delocalized around the negatively electrostatic molecular potential. For the present [C_2S_4; e^+] system, characteristics of the electronic structure related to the positron attatchement may help better understanding of the positron density distribution: We evaluated the electron density difference $\Delta\rho^e(\boldsymbol{r})$ induced by the positron attachment to C_2S_4, given as

$$\Delta\rho^e(\boldsymbol{r}) = \rho^e\left(\boldsymbol{r};[C_2S_4;e^+]\right) - \rho^e\left(\boldsymbol{r};[C_2S_4]\right), \tag{12}$$

where $\rho^e(\boldsymbol{r};[X])$ is the total electron density for the system X at the equilibrium nuclear geometry. In order to figure out the difference on properties for HF and CI, we here used $\rho^e(\boldsymbol{r};[CS_2])$ calculated by HF, and obtained $\rho^e(\boldsymbol{r};[X])$ using $\rho^e\left(\boldsymbol{r};[C_2S_4;e^+]\right)$ calculated by both HF and CI. Using the HF density for $\rho^e\left(\boldsymbol{r};[C_2S_4;e^+]\right)$ resulted in $|\Delta\rho^e(\boldsymbol{r})| < 10^{-7} e^- \cdot \text{bohr}^{-3}$ at a maximum. This means that in the HF level of the theory, significant relaxation due to the positron attachment does not occur. In contrast, in the CI level, as shown in Figure 1 (b), the electron density depletion $\Delta\rho^e(\boldsymbol{r}) < 0$ (blue isosurfaces) can be found in the vicinity of all sulfur atoms in the outer region, while the density enhancement $\Delta\rho^e(\boldsymbol{r}) > 0$ (red isosurfaces) can be found in the inner region of the C_2S_4 cluster. In particular, significantly increased electron density around the CC internuclear axis shows the partial polarization as favored in attracting a positron, which can be reproduced by inclusion of the electron-positron correlation effect via the CI level calculation.

According to our evaluation for the resonant positron kinetic energy K_ν from a rough treatment by $PA_\nu \sim PA(\boldsymbol{Q}_{eq})$ in Eq.(1) as a crude approximation, where non-degenerate four vibrational modes are assumed, two IR active modes for C_2S_4 as the first candidates for the vibrational resonance, $\nu = 4572$ and 4601 cm^{-1},

Table 2 The equilibrium geometries, the electrostatic constants, and the positron affinities for the monomer CS_2 and the dimer C_2S_4. The equilibrium CS and CC distances, R_{CS} and R_{CC}, are given in units of Å, and the intermolecular binding interaction energy E_{int} is shown in units of kcal/mol only for C_2S_4. The dipole moment μ and the polarizability α are given in units of debye and $bohr^3$ respectively. q_C and q_S show charges in units of electrons for carbon and sulfur atoms, respectively, obtained by the natural population analysis. PA^{HF} and PA^{CI} are positron affinities obtained by HF and CI, respectively, and are shown in units of meV.

Species	Symmetry	R_{CS}	θ_{SCS}	R_{CC}	E_{int}	μ	α	q_C	q_S	PA^{HF}	PA^{CI}
CS_2[a]	$D_{\infty h}$	1.56	180	–	–	0	49.6	−0.278	0.139	*unbound*	*unbound*
C_2S_4	D_{2d}	1.57	179.6	3.65[b]	2.07[b]	0	99.1	−0.256	0.128	*unbound*	46.18

[a] All data for the monomer from Reference [25]
[b] Estimation by the CCSD calculation in this work

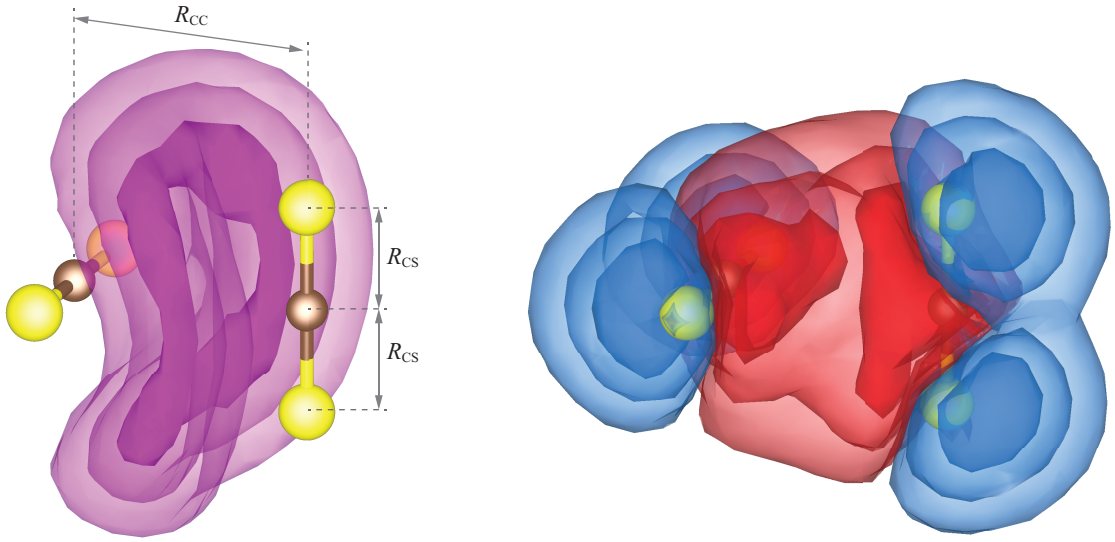

(a) Positron density (b) Electron density difference induced by positron attachment

Fig. 1 Positron density (a) and electron density difference induced by the positron attachment (b) for the $[C_2S_4; e^+]$ system. For (a), purple isodensity surfaces with 90%, 75%, and 60% of the maximum density 2.065×10^{-4} $e^+ \cdot bohr^{-3}$ are enclosed from inner to outer, while for (b), isodensity surfaces with $\Delta\rho^e(\boldsymbol{r}) = 1.5 \times 10^{-4}$, 5×10^{-5}, and 1×10^{-5} $e^- \cdot bohr^{-3}$ are shown by deep-to-light red colors, and those with $\Delta\rho^e(\boldsymbol{r}) = -1.5 \times 10^{-4}$, -5×10^{-5}, and -1×10^{-5} $e^- \cdot bohr^{-3}$ are shown by deep-to-light blue colors. In both (a) and (b), two carbon atoms separated by $R_{CC} = 3.65$ Å are shown by brown balls, and sulfur atoms connected to the central carbon atoms with the bond distance $R_{CS} = 1.57$ Å for each CS_2 unit are shown by yellow balls.

give $K_\nu = 141$ and 145 meV, respectively. These are still far from the estimated experimental value of $K_\nu = 115$ meV. In addition, IR inactive modes with the lowest vibrational energies, $\nu = 4390$ and 4410 cm^{-1}, give closer values, $K_\nu = 119$ and 120 meV, respectively, but slightly higher in compared to the experimental value. For more precise results, we evaluate the vibrational averaged PA and simulate the vibrational Feshbach resonance by taking account of the molecular vibrational effect in the following section.

4.2 Vibrational averaged positron affinity

Table 3 shows vibrational state quantum numbers n_is PA$_\nu$, μ_ν, α_ν, and K_ν for the lowest energy vibrational states arising from the fundamental tones, the overtones, and the over-combination tones of the IR inactive modes ν_1, ν_9, ν_{10}, and the IR active modes ν_{11}, ν_{12}. In our VSCF results for E_ν, the vibrational excitation energies $\Delta E_\nu = 1523$ cm^{-1} for $n_{12} = 0 \to 1$ and $\Delta E_\nu = 1552$ cm^{-1} for $(n_1, n_{12}) = (0,0) \to (1,1)$ are consistent with the corresponding experimentally measured IR spectra, 1533 and 1546 cm^{-1} [26], respectively. These show only error bars of approximate 0.5%, so that it is reasonable to be used for the vibrational averaging calculations.

In compared to the PA value of equilibrium geometry PA($\boldsymbol{Q}_{\rm eq}$) = 46.18 meV for the equilibrium state shown in Table 2, PA$_\nu$s increase to 54.7 meV for the ground and first three excited vibrational states and to about 63.5 meV for the last two vibrationally excited states. Using Eq. (1) with these PA$_\nu$, we can predict a few resonant peaks with in the ranges of $K_\nu = 111$–114 and 125–128 meV, which can be extremely close to the estimated experimental value of 115 meV in compared to the same analytical result $K_\nu = 5.02$ meV for the CS_2 monomer[25]. Considering the increase of PA due to the vibrational effect as ΔPA$_\nu$ = PA$_\nu$ − PA($\boldsymbol{Q}_{\rm eq}$), a major contribution to ΔPA$_\nu$, which can be obtained as ΔPA$_\nu = 9.5$ meV, is already gained in the vibrational ground state lying at $E_\nu = 3049$ cm^{-1}. In addition, there are small but significant contributions up to about ΔPA$_\nu = 14$ meV via the excitations of ν_9, ν_{10}, and ν_{12} in the vibrational excited states lying at $E_\nu = 4390$, 4410, and 4572 cm^{-1} in order to obtain the closest K_ν to the experimental value. Therefore, it may be indispensable to elucidate the mechanism of the vibrational enhancement of PA in terms of contributions from the ground state normal mode vibrations as well as the excited vibrational modes.

In order to figure out the detailed mechanism of the vibrational effect particularly for the vibrational ground state, we analyzed changes of PA, μ, and α with respect to the normal mode vibrational coordinates $\boldsymbol{Q}$. For the ground vibrational normal modes, we have found rough classification into three schemes; (A) PA$_{\nu_i}$ decreased or almost unchanged from PA($\boldsymbol{Q}_{\rm eq}$), (B) PA$_{\nu_i}$ increased without varying of μ, and (C) PA$_{\nu_i}$ significantly increased with increasing of μ (supplemental data can be available in Table S1 (ESI†)). As examples, in Figure 2 we show PA(Q_i), $\mu(Q_i)$, and $\alpha(Q_i)$ against displacements of the normal mode vibrational coordinates around the equilibrium ones, Q_i, for $i = 4$ (the CC intermolecular stretching), $i = 8$ (symmetric SCS bending vibration), and $i = 11, 12$ (degenerated asymmetric CS stretching) representing schemes (A), (B), and (C), respectively. In these figures, the upper and lower panels show PA(Q_i) and $|\psi_{\nu_i}(Q_i)|^2$, and $\mu(Q_i)$ and $\alpha(Q_i)$, respectively. For the CC stretching vibration shown in Figure 2 (a), $Q_i < 0$ and $Q_i > 0$ mean elongating and shrinking of the CC distance $R_{\rm CC}$ from the equilibrium distance, respectively, PA(Q_4) increases up to the local maximum of about 0.4 meV higher than PA($\boldsymbol{Q}_{\rm eq}$) = 46.18 meV at around $Q_4 \sim 0.5$ with increase of Q_4. Reducing PA by decrease of Q_4 reasonably shows that dissociation into individual CS_2 monomers reduces PA to zero for the equilibrium CS_2. In contrast, increasing behavior of PA due to increase of Q_4 in the range of the finite probability $|\psi_{\nu_4}|^2$ (shrinking of $R_{\rm CC}$) also shows that formation of C_2S_4 may be favored in enhancing the positron binding ability by change of the electronic structure. In this vibrational mode, as shown in the lower panel in Figure 2 (a), μ maintains zero, whereas α gradually decreases with increasing Q_4. For all vibrational states shown in Table 3, this vibrational mode with $\nu_4 = 0$ results in a negative contribution as PA$_{\nu_4} = 36.96$ meV. We have found that similarly, the A_1 symmetric CS stretching mode $i = 10$ negatively contributes to the vibrational averaged PA for the vibrational ground state (see Table S1 (ESI†)), although that is very small and PA$_{\nu_{10}}$ is almost the same to PA($\boldsymbol{Q}_{\rm eq}$).

For the vibrational mode $i = 8$ shown in Figure 2 (b), increasing of PA can be found with displacements Q_8 onto both directions in the range of finite probability $|\psi_{\nu_8}|^2$. On this vibrational mode, μ does not change but α increases due to the symmetric geometrical change with respect to the center of the CC internuclear axis. The same trend can be found in both the rotational-twisting mode ν_1 (see Figure S3 provided in ESI†). For the asymmetric CS stretching vibrations $i = 11$ (and 12) shown in Figure 2 (c), great increasing of PA by about few tens of meV is found in the range of finite $|\psi_{\nu_{11}}|^2$ (note that only for (c), vertical axes for PA and $|\psi_{\nu_i}|^2$ are shown in the different scaling to others). In this situation, although α slightly decreases, μ remarkably increases in almost proportional to the displacement Q_{11} onto both directions. Similar trends to this mode can be found in other vibrational modes as $i = 5$, 6, 7, and 9 containing SCS bending or CS stretching (see Figure S3 in ESI†for details), which are also asymmetric vibrational modes with respect to the center of the CC internulcear axis. However, for these modes, increases of PA and μ, which are

Table 3 The vibrational averaged positron affinity PA$_\nu$, the vibrational averaged dipole moment μ_ν, the vibrational averaged dipole polarizability α_ν, and the estimated resonant positron energy K_ν for each vibrational energy level ν of C_2S_4. The vibrational modes ν_i are defined in Table 1, and all of the other omitted vibrational quantum numbers for $i = 2$–8 are zeros. The vibrational energy levels E_ν are given in units of cm^{-1}, both PA$_\nu$ and K_ν are given in units of meV, and μ_ν and α_ν are given in units of debye and bohr^3 respectively.

$n_1, n_9, n_{10}, n_{11}, n_{12}$	E_ν	PA$_\nu$	μ_ν	α_ν	K_ν
(0, 0, 0, 0, 0)	3049	54.7	0.74	99.5	–
(0, 1, 1, 0, 0)	4390	54.7	0.74	99.7	111
(0, 0, 2, 0, 0)	4390	54.7	0.74	99.7	111
(0, 2, 0, 0, 0)	4410	54.5	0.74	99.6	114
(0, 0, 0, 0, 1)	4572	63.4	1.11	99.6	125
(1, 0, 0, 0, 1)	4601	63.5	1.11	99.7	128

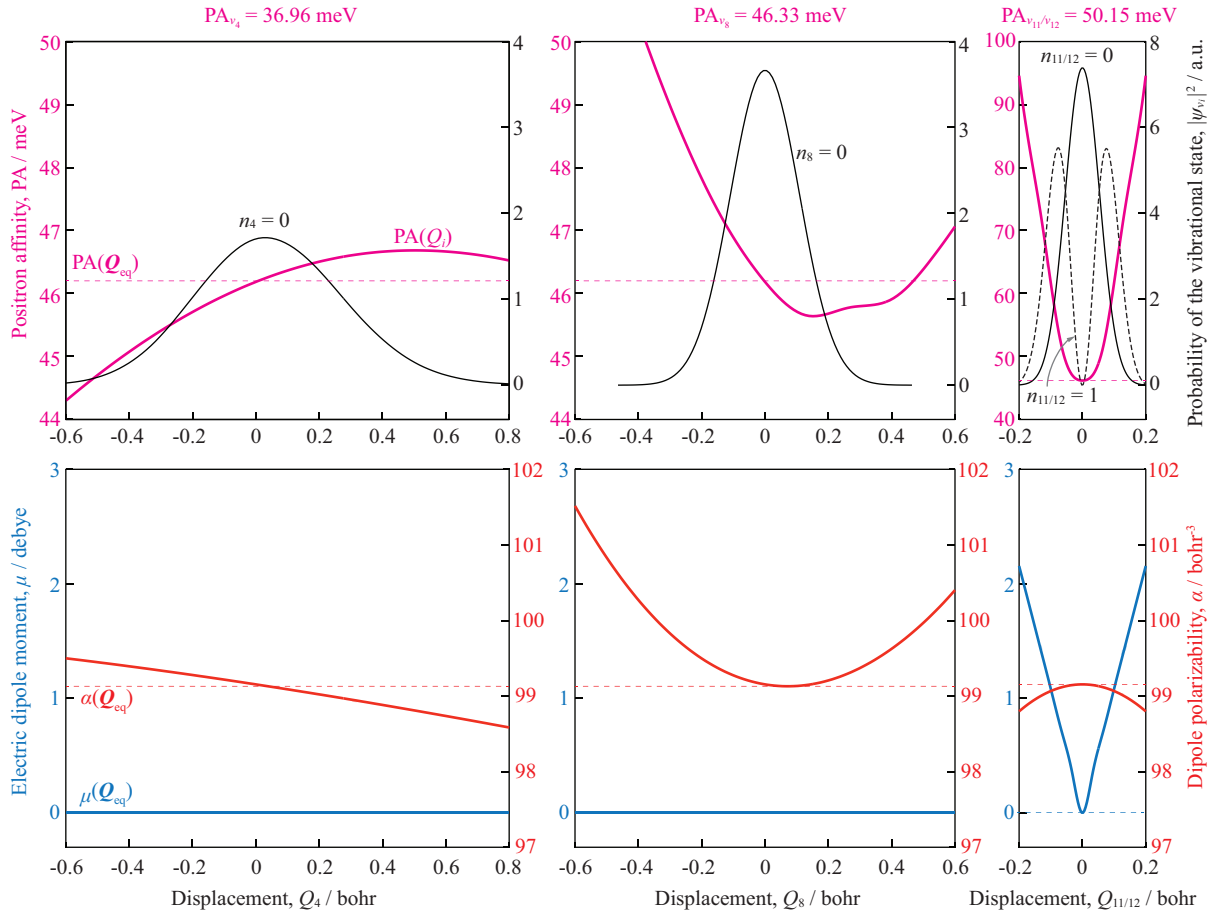

(a) On CC stretching vibration ($i = 4$)

(b) On symmetric SCS bending vibration ($i = 8$)

(c) On asymmetric CS stretching vibration (i =11 and 12)

Fig. 2 The probabilities of the vibrational states, the positron affinities, the dipole moments, and the dipole polarizabilities as functions of the normal mode vibrational coordinates Q_i for (a) $i = 4$, (b) $i = 8$, and (c) $i = 11$ and 12. Horizontal axes are given as displacements from the equilibrium coordinates in units of bohr.

less than 0.5 meV and 0.1 debye, respectively, are very small in compared to $i = 11$ and 12.

Exceptionally, only for the vibrational mode $i = 2$ and 3 (degenerated wagging motions of CS_2 units), we found that PA is reduced with the vibrational displacement and shows negative correlations with both μ and α (see Figure S3 in ESI†). In such vibrational motions, the positron binding is considered to be rather weaken due to the repulsive Coulomb interaction with the partially positively charged sulfur atoms. However, this contribution is comparatively small and not large enough to be dominant. Thus, in the case of [C_2S_4; e^+] system, we confirmed two effective mechanisms of the vibrationally enhanced positron capture in the vibrational ground state related to the vibrational normal modes; the first one can be regarded as positive correlations between PA and α as seen in the dependence on Q_8, and the second one can be regarded as positive correlations between PA and μ as seen in the dependence on Q_{11}. For the [C_2S_4; e^+] system, the latter mechanism has the especially dominant contribution to the increased PA in the vibrational ground state as well as first two or three vibrational excited states shown in Table 3.

Similar analytical result for vibrationally enhanced PA was seen in the case study for [CS_2; e^+][25]. Referring to the results for CS_2, the largest increasing of PA (almost equivalent to PA_ν for CS_2) of about 2–5 meV can be found in the fundamental tones, the first overtones, and the first combination tones associated with the asymmetric CS stretching vibration mode, which also exhibit increasing of μ_ν by 1–2 debye. Assuming PA_ν to have a linear dependence at least on μ_ν; namely, $PA_\nu \sim a\mu_\nu + b$ with constants a and b as presented by Takeda *et al.*[25], the [CS_2; e^+] system showed $a = 4.78$ meV/debye, while the [C_2S_4; e^+] system showed $a = 23.78$ meV/debye.

In Table 3, in particular, $K_\nu = 114$ meV arising from the vibrational excitation by the first overtone $n_9 = 2$ for the B_2 symmetric CS stretching vibrational mode is the closest energy to the experimental value. This results from the peak shift by the vibrational energy for the vibrational excited state with $n_9 = 2$ lying about 20 cm^{-1} above both of the combination tone $(n_9, n_{10}) = (1,1)$ and the overtone $(n_9, n_{10}) = (0,2)$, although these PA_νs are almost equal to each other. Such higher excited vibrational energy level for $n_9 = 2$ differentiated from $(n_9, n_{10}) = (1,1)$ and $(0,2)$ is clearly caused by its anharmonicity. These lower vibrational excited states giving resonant positron kinetic energies of 111–114 meV can be considered to have significant contributions to the positron capture in the vibrational resonance, despite IR inactiveness. Possibilities of contributions from IR inactive modes were also suggested in the case studies for the vibrational resonant positron captures on 1,2-trans-dichloroethylene and tetrachloroethylene with non-dipole interaction[12]. On the other hand, $K_\nu = 125$ meV, which is slightly higher than the experimental value, arises from the vibrational excitation by the fundamental tone $n_{12} = 1$ for the asymmetric CS stretching vibrational mode. This increased PA_ν can be considered to be yielded by the effective enhancement by the probability of the vibrational state, as illustrated by $n_{12} = 1$ in Figure 2 (c).

5 Conclusions

We have investigated the positron binding ability by taking the vibrational effect into account for the [C_2S_4; e^+] system using both the configuration interaction level and Hartree-Fock level of multi-component molecular orbital method combined with the self-consistent field level of vibrational variational Monte Carlo method. We found that the equilibrium structure of C_2S_4 can have the positronic bound state with the positron affinity (PA) of 46.18 meV in configuration interaction level while 0 meV in Hartree-Fock level, where the electron-positron correlation effect as well as the electronic structure of C_2S_4 is crucial to reproduce the positive PA value. By calculating the vibrational averaged PA, we obtained that [C_2S_4; e^+] can posses a few peaks corresponding to the resonant positron kinetic energies in the range of 111–125 meV closing to the experimentally observed value estimated to be 115 meV. The calculation result was also drastically improved compared to our previous study on the [CS_2; e^+] system in which the vibrational averaged PA was underestimated and resonance positron kinetic energies K_ν = 190 meV. Our analytical results for vibrational averaged properties showed that PA can be effectively increased by increased dipole moment along several asymmetric SCS bending modes, and by increased dipole polarizability on the symmetric CS stretching or SCS bending modes. The former mechanism for infrared active modes yields the dominant contribution of the vibrationally enhanced PA via the ground vibrational modes, while the latter one for infrared inactive modes have non-negligible contribution, particularly, via the excited vibrational modes. These effects for [C_2S_4; e^+] was also verified to be stronger than that for [CS_2; e^+].

Conflicts of interest

There are no conflicts to declare.

Acknowledgements

This work was partly supported by Grants-in-Aid for Scientific Research (KAKENHI) of the Ministry of Education, Culture, Sports, Science and Technology (MEXT) (Grant Nos. 18H01945, 19H05063, and 21H00026 for M.T., and Grant Nos. 18K05041 and 21K04983 for Y.K.). The computations were partly performed using the resources provided by the Research Center for Computational Science (RCCS), Okazaki, Japan.

References

1 P. Indelicato, G. Chardin, P. Grandemange, D. Lunney, V. Manea, A. Badertscher, P. Crivelli, A. Curioni, A. Marchionni, B. Rossi, A. Rubbia, V. Nesvizhevsky, D. Brook-Roberge, P. Comini, P. Debu, P. Dupré, L. Liszkay, B. Mansoulié, P. Pérez, J.-M. Rey, B. Reymond, N. Ruiz, Y. Sacquin, B. Vallage, F. Biraben, P. Cladé, A. Douillet, G. Dufour, S. Guellati, L. Hilico, A. Lambrecht, R. Guérout, J.-P. Karr, F. Nez, S. Reynaud, C. I. Szabo, V.-Q. Tran, J. Trapateau, A. Mohri, Y. Yamazaki, M. Charlton, S. Eriksson, N. Madsen, D. P. van der Werf, N. Kuroda, H. Torii, Y. Nagashima, F. Schmidt-Kaler, J. Walz, S. Wolf, P.-A. Hervieux, G. Man-

fredi, A. Voronin, P. Froelich, S. Wronka and M. Staszczak, *Hyp. Int.*, 2014, **228**, 141–150.
2 P. Peŕez, D. Banerjee, F. Biraben, D. Brook-Roberge, M. Charlton, P. Cladé, P. Comini, P. Crivelli, O. Dalkarov, P. Debu, A. Douillet, G. Dufour, P. Dupré, S. Eriksson, P. Froelich, P. Grandemange, S. Guellati, R. Guérout, J. M. Heinrich, P.-A. Hervieux, L. Hilico, A. Husson, P. Indelicato, S. Jonsell, J.-P. Karr, K. Khabarova, N. Kolachevsky, N. Kuroda, A. Lambrecht, A. M. M. Leite, L. Liszkay, D. Lunney, N. Madsen, G. Manfredi, B. Mansoulié, Y. Matsuda, A. Mohri, T. Mortensen, Y. Nagashima, V. Nesvizhevsky, F. Nez, C. Regenfus, J.-M. Rey, J.-M. Reymond, S. Reynaud, A. Rubbia, Y. Sacquin, F. Schmidt-Kaler, N. Sillitoe, M. Staszczak, C. I. Szabo-Foster, H. Torii, B. Vallage, M. Valdes, D. P. van der Werf, A. Voronin, J. Walz, S. Wolf, S. Wronka and Y. Yamazaki, *Hyp. Int.*, 2015, **233**, 21–27.
3 L. D. Hulett, Jr, D. L. Donohue, J. Xu, T. A. Lewis, S. A. McLuckey and G. L. Glish, *Chem. Phys. Lett.*, 1993, **216**, 236–240.
4 F. Tuomisto and I. Makkonen, *Rev. Mod. Phys.*, 2013, **85**, 1583–1631.
5 I. H. Shon, M. J. O'Doherty and M. N. Maisey, *Semin. Nucl. Med.*, 2002, **32**, 240–271.
6 R. L. Wahl, B. A. Siegel, R. Edward Coleman and C. G. Gatsonis, *J. Clin. Oncol.*, 2004, **22**, 277–285.
7 J. A. Young and C. M. Surko, *Phys. Rev. A*, 2008, **77**, 052704.
8 J. A. Young and C. M. Surko, *Phys. Rev. A*, 2008, **78**, 032702.
9 A. C. L. Jones, J. R. Danielson, J. J. Gosselin, M. R. Natisin and C. M. Surko, *New J. Phys.*, 2012, **14**, 015006.
10 J. R. Danielson, A. C. L. Jones, J. J. Gosselin, M. R. Natisin and C. M. Surko, *Phys. Rev. A*, 2012, **85**, 022709.
11 C. M. Surko, J. R. Danielson, G. F. Gribakin and R. E. Continetti, *New J. Phys.*, 2012, **14**, 065004.
12 M. R. Natisin, J. R. Danielson, G. F. Gribakin, A. R. Swann and C. M. Surko, *Phys. Rev. Lett.*, 2017, **119**, 113402.
13 G. F. Gribakin, *Phys. Rev. A*, 2000, **61**, 022720.
14 G. F. Gribakin and C. M. R. Lee, *Phys. Rev. Lett.*, 2006, **97**, 193201.
15 J. Mitroy, M. W. J. Bromley and G. G. Ryzhikh, *J. Phys. B: At., Mol. Opt. Phys.*, 1999, **32**, 2203–2214.
16 A. R. Swann and G. F. Gribakin, *J. Chem. Phys.*, 2020, **153**, 184311.
17 G. G. F, J. A. Young and C. M. Surko, *Rev. Mod. Phys.*, 2010, **82**, 2557–2607.
18 H. Chojnacki and K. Strasburger, *Mol. Phys.*, 2006, **104**, 2273–2276.
19 Y. Kita, R. Maezono, M. Tachikawa, M. Towler and R. J. Needs, *J. Chem. Phys.*, 2009, **131**, 134310.
20 M. Tachikawa, Y. Kita and R. J. Buenker, *Phys. Chem. Chem. Phys.*, 2011, **13**, 2701–2705.
21 J. A. Charry, J. Romero, M. T. do Nascimento Varella and A. Reyes, *Phys. Rev. A: At., Mol., Opt. Phys.*, 2014, **89**, 052709.
22 M. Nummela, H. Raebiger, D. Yoshida and M. Tachikawa, *J. Phys. Chem. A*, 2016, **120**, 4037–4042.
23 Y. Kita and M. Tachikawa, *Chem. Phys. Lett.*, 2009, **482**, 201–206.
24 J. R. Danielson, J. J. Gosselin and C. M. Surko, *Phys. Rev. Lett.*, 2010, **104**, 233201.
25 Y. Takeda, Y. Kita and M. Tachikawa, *Eur. Phys. J. D*, 2016, **70**, 132.
26 M. Rezaei, J. Norooz Oliaee, N. Moazzen-Ahmadi and A. R. W. McKellar, *J. Chem. Phys.*, 2011, **134**, 144306.
27 A. J. Barclay, K. Esteki, K. H. Michaelian, A. R. W. McKellar and N. Moazzen-Ahmadi, *J. Chem. Phys.*, 2019, **150**, 144305.
28 J. K. G. Watson, *Mol. Phys.*, 1968, **15**, 479–490.
29 M. Tachikawa, K. Mori, K. Suzuki and K. Iguchi, *Int. J. Quantum Chem.*, 1998, **70**, 491–501.
30 L. E. McMurchie and E. R. Davidson, *J. Comput. Phys.*, 1978, **26**, 218–231.
31 I. Shavitt, *The Unitary Group for the Evaluation of Electronic Energy Matrix Elements*, Springer, Berlin, Hinze, Jürgen edn, 1981.
32 B. L. Hammond, W. A. Lester, Jr and P. J. Reynolds, *Monte Carlo Methods in Ab Initio Quantum Chemistry*, World Scientific Publishing Company, 1994, vol. 1.
33 M. J. Frisch, G. W. Trucks, H. B. Schlegel, G. E. Scuseria, M. A. Robb, J. R. Cheeseman, G. Scalmani, V. Barone, G. A. Petersson, H. Nakatsuji, X. Li, M. Caricato, A. V. Marenich, J. Bloino, B. G. Janesko, R. Gomperts, B. Mennucci, H. P. Hratchian, J. V. Ortiz, A. F. Izmaylov, J. L. Sonnenberg, D. Williams-Young, F. Ding, F. Lipparini, F. Egidi, J. Goings, B. Peng, A. Petrone, T. Henderson, D. Ranasinghe, V. G. Zakrzewski, J. Gao, N. Rega, G. Zheng, W. Liang, M. Hada, M. Ehara, K. Toyota, R. Fukuda, J. Hasegawa, M. Ishida, T. Nakajima, Y. Honda, O. Kitao, H. Nakai, T. Vreven, K. Throssell, J. A. Montgomery, Jr., J. E. Peralta, F. Ogliaro, M. J. Bearpark, J. J. Heyd, E. N. Brothers, K. N. Kudin, V. N. Staroverov, T. A. Keith, R. Kobayashi, J. Normand, K. Raghavachari, A. P. Rendell, J. C. Burant, S. S. Iyengar, J. Tomasi, M. Cossi, J. M. Millam, M. Klene, C. Adamo, R. Cammi, J. W. Ochterski, R. L. Martin, K. Morokuma, O. Farkas, J. B. Foresman and D. J. Fox, *Gaussian 16 Revision C.01*, 2016, Gaussian Inc. Wallingford CT.
34 S. Carter, S. J. Culik and J. M. Bowman, *J. Chem. Phys.*, 1997, **107**, 10458.
35 Y. Kita and M. Tachikawa, *Eur. Phys. J. D*, 2014, **68**, 116.
36 D. J. Tildesley and P. A. Madden, *Mol. Phys.*, 1981, **42**, 1137–1156.